Wideband Frequency-Domain Characterization of FR-4 and Time-Domain Causality

Djordjevi, A.R.; Biljie, R.M.; Likar-Smiljanic, V.D.; Sarkar, T.K.; Sch. of Electr. Eng., Belgrade Univ.

Wideband Frequency-Domain Characterization of FR-4 and Time-Domain Causality

Antonije R. Djordjević, Radivoje M. Biljić, Vladana D. Likar-Smiljanić[1], and Tapan K. Sarkar[2]

Abstract - **FR-4 is one of the most widely used dielectric substrates in the fabrication of printed circuits for fast digital devices. This material exhibits substantial losses and the loss tangent is practically constant over a wide band of frequencies. This paper presents measured data for the complex permittivity of this material from power frequencies up to the microwave region. In addition it gives simple closed-form expressions that approximate the measured data and provide a causal response in the time domain.**

I. Introduction

One of the most widely used substrates in the fabrication of printed-circuit boards for fast digital circuits is FR-4. It is used both for classical boards and for multilayered boards. This low-cost composite material consists of glass fibers embedded in an epoxy resin.

For modern digital circuits, signal spectra are wide and they extend deeply into the microwave region (of the order of several GHz). For a successful modeling and design of signal interconnects, it is important to know frequency variations of the dielectric parameters. This paper presents relatively simple mathematical expressions that approximate measured results for the complex relative permittivity of FR-4 in a wide frequency band. These expressions are such that they automatically provide a causal response in the time domain.

The paper does not provide a complete characterization of the material properties. Hence, we do not consider the influence of the contents of the glass fibers, temperature, humidity, pressure, etc., and we also neglect anisotropic properties of FR-4.

The complex relative permittivity of FR-4 in the frequency domain (ε_r) is separated into the real (ε') and imaginary (ε'') parts in the usual way, as

$$\varepsilon_r = \varepsilon' - j\varepsilon'' = \varepsilon'(1 - j\tan\delta). \tag{1}$$

Manufacturers usually give the complex permittivity only at a relatively low frequency (typically, 50 or 60 Hz, or 1 MHz). A wide range for the real part can be found in their data, $\varepsilon' = 4.2 - 5.5$. The material has significant losses and the loss tangent ($\tan\delta$) is of the order of 0.02 in a broad frequency range. This corresponds to the imaginary part of the complex permittivity that is on the order of $\varepsilon'' = 0.1$.

Professor Dr. Antonije R. Djordjević
University of Belgrade, School of Electrical Engineering
P.O. Box 35-54, 11120 Belgrade, Yugoslavia
Fax: +381 11 324 8681, Telex: 71071 (YUETF), Phone: ++ 381 11 3370 101
Electronic mail: edjordja@ubbg.etf.bg.ac.yu

[1] A. R. Djordjević, R. M. Biljić, and V. D. Likar-Smiljanić are with the School of Electrical Engineering, University of Belgrade, 11120 Belgrade, Yugoslavia

[2] T. K. Sarkar is with the Department of Computer Science and Electrical Engineering, Syracuse University, Syracuse, N.Y. 13244-1240

In Section II experimental data are presented for the complex permittivity of FR-4 in a wide frequency range, from power frequencies up to about 12 GHz. These data show that ε' slowly decreases with frequency, ε" is almost constant, and the resulting loss tangent is also practically independent of frequency. In Section III, we derive closed-form approximations for the frequency variations of the complex permittivity that ensure a causal response in the time domain. Finally, Section IV applies derived formulas to the analysis of wave propagation in FR-4.

II. Experimental Evaluation of Dielectric Parameters

A variety of techniques has been proposed that can be used for measurement of the complex permittivity of dielectric substrates [1,2]. Our focus here is on FR-4 and similar substrates, whose thickness is in the range 0.2-3 mm (8-120 mils), the relative permittivity about 5, and the loss tangent about 0.02. We quote some of the methods, without trying to make an exhaustive list.

- The substrate with the metallization on both faces can be regarded as a parallel-plate capacitor and its admittance can be measured using impedance bridges, impedance meters, or other devices [3]. Hence, the complex capacitance and the complex permittivity can be calculated. This non-destructive method can be used in the frequency range from about 10 Hz up to 100 MHz.
- The substrate, the standard metallization on both faces, and an added metallization on the rim form a cavity resonator [4]. A network analyzer can be weakly coupled to the cavity at two locations. The resonant frequencies and the quality factor of the resonator can be measured. Hence, the complex permittivity can be calculated. This technique is practically non-destructive, and it can be used for frequencies of the order of 0.1-10 GHz, depending on the board size and permittivity.
- A resonator can be printed on the substrate (e.g., a half-wavelength open-ended microstrip line or a ring resonator) and a transmission line coupled to it [5]. The complex permittivity can be extracted from measured data for the scattering parameters of the line, i.e., from the notch in the transfer function. This technique can be used for frequencies of the order of 0.1-10 GHz. A reliable numerical model of a microstrip transmission line is required, including the open-end effect for the half-wavelength resonator.
- A single transmission line can be printed on the substrate (e.g., a microstrip line) and its scattering parameters can be measured. The complex permittivity can be extracted in a variety of ways. This technique also requires a reliable numerical model of the transmission line, and it can be used for frequencies of the order of 0.01-10 GHz. This simple idea is not advocated in the literature, and we were able to trace only one related paper [6].
- A dielectric sample (with no metallization on it) can be inserted into an air coaxial line or a waveguide [7-13]. From the measured scattering parameters, the complex permittivity can be evaluated by closed-form formulas or iteratively, depending on the method. There exist various approaches, based on measuring the reflection, transmission, or both. The reflection can be measured when the dielectric sample is backed by a short circuit or by a matched line or waveguide. These techniques are suitable for the frequency range of the order of 0.1-30 GHz.

In methods that involve a metallization on the substrate, usually there is a problem to distinguish between losses in the conductors and in the substrate. The problem is primarily due to the surface roughness of the conductors, as it substantially increases the conductor losses. In the case of FR-4, the dielectric losses usually dominate at microwave frequencies, so that an accurate characterization of the conductor losses is not crucial.

The purpose of this paper is to characterize FR-4 in a wide frequency range that is important for digital printed-circuit boards. This range starts from about 1 MHz and goes up to about 10 GHz. However, for completeness, we have extended the range down to power frequencies, more precisely to 10 Hz. This wide frequency range can be spanned only by combining several techniques. We have used methods that overlap in frequency ranges in order to compare several sets of results. In all cases, a substrate of a nominal thickness of 62 mils (1.575 mm) was used, and all samples were made from the same board. The thickness of the copper was 35 μm (1 oz per square foot). Variations of the substrate thickness over the board were on the order of 0.1 mm. The substrate was at room temperature.

The lower frequency band (10 Hz-50 MHz) was covered by the parallel-plate capacitor technique. The admittance of the metallized FR-4 plate was measured using HP 4800 and HP 4291A impedance meters. Several plate sizes were used. A larger size was required for the low end (to obtain a sufficiently high capacitance), and a smaller size was required for the high end (to avoid the propagation effects in the substrate).

We have developed a simple transmission-line method to cover the upper frequency band (50 MHz-12 GHz). A microstrip line was fabricated on the FR-4 substrate. The characteristic impedance of the line was close to 50 Ω (trace width 3.0 mm), and the line length was 300 mm. The line was carefully terminated in two SMA connectors to facilitate deembedding. The scattering parameters of the line were measured at a set of frequencies, using the HP 8510B network analyzer. Thereafter, using program Touchstone [14], the measured data were emulated by optimizing the relative permittivity and the loss tangent of the substrate at each frequency. The Touchstone model includes the conductor losses and the dispersion of the quasi-TEM mode. This technique works well up to about 12 GHz. Above this frequency, higher-order modes and radiation from the microstrip line come into effect, thus disabling the measurements.

Our technique, described above, has several advantages over the method described in [6]. First, the method of [6] is valid only for lines with a homogeneous dielectric. Therefore, they had to use a stripline, which is more difficult for fabrication than a microstrip line used in our technique. Second, the method of [6] does not treat the conductor losses, but rather includes all the losses into the imaginary part of the complex permittivity. Therefore, our method is to be expected to yield more accurate results, in particular for dielectrics with medium to lower losses. Note that the key equations in [6] contain typographic errors, which should be corrected before applying the method.

For frequencies near 10 GHz, three additional techniques were used based on X-band waveguide measurements, with the purpose to provide some independent data for checking. The first technique was to measure the reflection coefficient of a short-circuited rectangular waveguide [7,8], where a dielectric slab was inserted next to the short circuit. The reflection coefficient was measured automatically, using the HP 8410C network analyzer, and manually, using the HP X809B slotted waveguide. The measured results were then emulated on a numerical model (based on direct and reflected dominant waveguide modes), by optimizing the complex permittivity of the slab using an improved version of the algorithm from [15]. In the second technique [9,10], the dielectric slab was backed by a matched waveguide, the reflection coefficient was measured using the network analyzer, and the results were again emulated using a numerical model. Finally, the third technique was based on positioning the slab in a through waveguide, measuring the scattering parameters, and explicitly evaluating the complex permittivity as described in [11-13]. Thereby, the relative permeability of the slab was *a priori* taken to be 1, as in [13], which simplifies the extraction of the complex permittivity. Raw results (i.e., without smoothing) obtained by these three techniques are shown in Figure 1. This figure also shows the complex permittivity as obtained from the transmission-line method described above. Obviously, the simple transmission-line method yields smoothest and physically most logical data. The estimated error bound is 2% for ε' and 5% for ε''. This bound takes into account the measurement errors on the network analyzer and accuracy of the numerical model used to extract dielectric parameters. Relatively reliable data for ε' were also obtained from the first two waveguide techniques, and the results for ε' are within 5% from the transmission-line data, except at the ends of the frequency band. A more detailed comparison of the waveguide methods is beyond the scope of this paper.

Figure 2 shows the relative permittivity of FR-4 in a wide frequency band, from 10 kHz to 12 GHz, as a compilation of results obtained by the parallel-plate and the transmission-line methods. The results are not smoothed nor are potentially bad points removed from the data sets. The estimated absolute error bound in the whole frequency band is 0.2 for ε' and 0.02 for ε''. The real part (ε') decays with frequency. In particular, between 10 kHz and 10 GHz, the decay has an almost uniform slope of about 0.14 per decade. The imaginary part (ε'') and the loss tangent have relatively small variations in this band. Going towards very low frequencies, the imaginary part increases due to the finite conductivity of the material, which confirms the results obtained by d.c. measurement of the parallel-plate capacitor resistance.

III. Closed-Form Formulas for Dielectric Parameters

There exist several polarization mechanisms of dielectrics [16,17], when they are subject to an external electric field. Depending on the kind of charged particles that are involved, there are the electron polarization, the dipole polarization, the ion polarization, and the macrodipole polarization. The polarization can further be classified as elastic (e.g., the electron polarization), relaxation (where the thermal motion of the particles has an important role), and the space-charge polarization (for

inhomogeneous dielectrics). Another classification distinguishes the intrinsic polarization, the polarization due to impurities, and the polarization of inhomogeneous dielectrics.

Each polarization mechanism has associated dielectric losses (described by ε'') and variations of the real part of the relative permittivity (ε'). In the simplest models usually found in the literature, for each mechanism, the variations of ε' and ε'' are localized in a relatively narrow frequency range. For example, the complex relative permittivity associated with the relaxation polarization is mathematically described as

$$\varepsilon_r(\omega) = \varepsilon'_\infty + \frac{\Delta\varepsilon'}{1+j\dfrac{\omega}{\omega_o}} \,, \tag{2}$$

where ε'_∞ is the (real part of) the relative permittivity at high frequencies, $\Delta\varepsilon'$ is the variation of the real part of relative permittivity, and ω_o is the angular frequency where the variations of the permittivity are centered. The peak of ε'' is $\Delta\varepsilon'/2$. As an example, Figure 2 shows the real and imaginary parts of the complex relative permittivity resulting from eqn. (2) for $\varepsilon'_\infty = 4.9$, $\Delta\varepsilon' = 0.28$, and $\omega_o = 2\cdot10^6\ \text{s}^{-1}$. These coefficients were obtained by fitting the measured data for FR-4 around 300 kHz.

The real and imaginary parts of the complex permittivity, defined by eqn. (2), satisfy the Kramers-Kronig relations, i.e., they yield a causal response in the time domain. In other words, the real and imaginary parts are related by the Hilbert transform. For a parallel-plate capacitor (of electrode surface area S and interelectrode separation d), eqn. (2) corresponds to the equivalent scheme shown in Figure 3(a), where $C_\infty = \varepsilon_0\varepsilon'_\infty\, S/d$, $C = \varepsilon_0\Delta\varepsilon'\, S/d$, and $1/R = \omega_0\varepsilon_0\Delta\varepsilon'\, S/d$.

The elastic polarization is described by more a complicated term, which corresponds to an equivalent *RLC* scheme. This term is a rational function that has a second-order polynomial (in terms of ω) in its denominator, and it yields a negative real part of the complex permittivity within a certain frequency band. Such a polarization mechanism is not visible in our experimental results, but it should be detectable in the infrared region and above.

It is well known that the loss tangent of FR-4 is relatively independent of frequency in a wide frequency range, but the authors were unable to trace in literature a physical explanation of the polarization mechanism of FR-4 that is responsible for such a behavior. However, our objective here is only to provide simple closed-form formulas that approximate the measured complex permittivity of FR-4, which are suitable for the numerical analysis of circuits made on this substrate.

Merely taking the loss tangent to be a constant (without having any variations in ε') would yield a non-causal response in the time domain [18,19]. Taking the loss tangent to be constant in a finite frequency range and zero otherwise, results in unnatural frequency variations of ε' required by the Hilbert transform to yield a causal response. Hence, other ways must be found to model the frequency variations of the complex permittivity of FR-4 and similar dielectric materials.

From the results in Figure 2, it can be seen that the complex permittivity of FR-4 cannot adequately be described by eqn. (2), because the decay of ε' in the experimental data is distributed over a wide frequency band, while the decay yielded by eqn. (2) is localized around ω_o. However, a good approximation of the experimental data may be obtained by summing several terms of the same form as in eqn. (2), i.e., by

$$\varepsilon_r(\omega) = \varepsilon'_\infty + \sum_{i=1}^{N} \frac{\Delta\varepsilon'_i}{1+j\dfrac{\omega}{\omega_i}} - j\frac{\sigma}{\omega\varepsilon_0} \,. \tag{3}$$

This amounts to assuming that there are several relaxation terms; each localized at a different angular frequency [17]. The last term in eqn. (3) corresponds to the volume conductivity (σ) of the dielectric. This term dominates at low frequencies, and in our case it is pronounced below about 20 Hz. The equivalent scheme for a parallel-plate capacitor, resulting from equation (3), is shown in Figure 3(b), where $C_\infty = \varepsilon_0\varepsilon'_\infty\, S/d$; $C_i = \varepsilon_0\Delta\varepsilon'_i\, S/d$, $1/R_i = \omega_0\varepsilon_0\Delta\varepsilon'_i\, S/d$, $i = 1,\ldots,N$; and $R_0 = d/\sigma S$.

The terms in eqn. (3) should be distributed over the frequency band of interest by appropriately selecting the angular frequencies $\omega_i, i = 1,\ldots,N$. The decay of the experimental results for ε', shown in Figure 2, is practically uniform versus the logarithm of the frequency in the band from

about 10 kHz to 10 GHz. Hence, these angular frequencies should be evenly distributed on a logarithmic scale in this band, and the coefficients $\Delta\varepsilon'_i$, $i = 1, \ldots, N$, should be on the same order of magnitude. Numerical experiments have shown that it is sufficient to take one term per decade. Such an approximation can yield a relatively uniform ε'', with less than 10% variations. Figure 4 shows the approximation for the experimental results obtained with $N=8$, $\varepsilon'_\infty = 4.20$, $\sigma = 80 \, \text{pS/m}$, and the following parameters of the sum in eqn. (3):

i	1	2	3	4	5	6	7	8
$\omega_i \, [\text{s}^{-1}]$	20 k	200 k	2 M	20 M	200 M	2 G	20 G	200 G
$\Delta\varepsilon'_i$	0.12	0.14	0.22	0.18	0.12	0.10	0.10	0.24

The approximation given by eqn. (3) automatically yields a causal response in the time domain, as it is a sum of terms each of which yields a causal response. A better fit than shown in Figure 4 can be obtained by taking more terms, as well as by a simultaneous fine-tuning of both ω_i and $\Delta\varepsilon'_i$.

An even simpler approximation can be deduced in the following way. We can increase the number of terms in eqn. (3), keeping the uniform spread of ω_i on the logarithmic scale. This increase reduces the oscillations of ε''. Let us assume that ε'' is approximately constant between $\omega_1 = 10^{m_1}$ (lower limit) and $\omega_2 = 10^{m_2}$ (upper limit). Let $\Delta\varepsilon'$ be the total variation of ε' between lower and the upper limit. This variation is assumed to be uniformly distributed over the logarithm of the frequency, so that $\dfrac{\Delta\varepsilon'}{m_2 - m_1}$ is the variation per decade. On the logarithmic scale, this means a linear decay of ε'. Hence, the terms in the sum in eqn. (3) are uniformly distributed on the logarithmic scale, i.e., the ratio ω_{i+1}/ω_i is constant. By taking an infinite number of terms, in the limit, the sum in eqn. (3) becomes

$$\sum_{i=1}^{N} \frac{\Delta\varepsilon'_i}{1 + j\dfrac{\omega}{\omega_i}} \rightarrow \frac{\Delta\varepsilon'}{m_2 - m_1} \int_{x=m_1}^{m_2} \frac{dx}{1 + j\dfrac{\omega}{10^x}} = \frac{\Delta\varepsilon'}{m_2 - m_1} \frac{\ln\dfrac{\omega_2 + j\omega}{\omega_1 + j\omega}}{\ln 10} . \tag{4}$$

For clarity, $\ln 10$ can be associated with the logarithm in the numerator to effectively get the logarithm for base 10. Alternatively, the constants m_1 and m_2 can be multiplied by $\ln 10$, thus becoming natural logarithms of the lower and upper angular frequency bounds, respectively.

The integral in eqn. (4) automatically yields a causal response in the time domain, as it is a sum (though infinite) of causal terms. The complex relative permittivity is now given by

$$\varepsilon_r(\omega) = \varepsilon'_\infty + \frac{\Delta\varepsilon'}{m_2 - m_1} \frac{\ln\dfrac{\omega_2 + j\omega}{\omega_1 + j\omega}}{\ln 10} - j\frac{\sigma}{\omega\varepsilon_o} . \tag{5}$$

For the frequency range where $\omega_1 \ll \omega \ll \omega_2$, the real part of the integral in (4) is

$$\text{Re}\left\{ \frac{\Delta\varepsilon'}{m_2 - m_1} \frac{\ln\dfrac{\omega_2 + j\omega}{\omega_1 + j\omega}}{\ln 10} \right\} = \frac{\Delta\varepsilon'}{m_2 - m_1} \frac{\ln\left|\dfrac{\omega_2 + j\omega}{\omega_1 + j\omega}\right|}{\ln 10} \approx \frac{\Delta\varepsilon'}{m_2 - m_1} \frac{\ln\dfrac{\omega_2}{\omega}}{\ln 10} , \tag{6}$$

and it linearly decays with the logarithm of the frequency, for $\Delta\varepsilon'/(m_2 - m_1)$ per decade, which matches well the experimental data. In the same frequency band, the imaginary part of the integral,

$$\text{Im}\left\{ \frac{\Delta\varepsilon'}{m_2 - m_1} \frac{\ln\dfrac{\omega_2 + j\omega}{\omega_1 + j\omega}}{\ln 10} \right\} = \frac{\Delta\varepsilon'}{m_2 - m_1} \frac{\arg\left\{\dfrac{\omega_2 + j\omega}{\omega_1 + j\omega}\right\}}{\ln 10} \approx \frac{\Delta\varepsilon'}{m_2 - m_1} \frac{-\dfrac{\pi}{2}}{\ln 10} , \tag{7}$$

is practically constant. Equation (7) also shows the relation between ε' and ε": the imaginary part of the complex permittivity (ε") equals $\dfrac{\pi/2}{\ln 10} \approx 0.682$ times the decay of ε' per decade. The resulting loss tangent gradually increases with frequency if $\sigma/(\omega\varepsilon_o)$ is negligibly small, because ε" is a constant and ε' slowly decays.

For frequencies below ω_1 or above ω_2, the imaginary part of the integral tends to zero, while the real part tends to be constant.

Figure 4 also shows the approximation for the experimental results obtained using eqn. (5), with $\varepsilon'_\infty = 4.27$, $\sigma = 80\,\text{pS/m}$, $\omega_1 = 10^4\,\text{s}^{-1}$ (i.e., $m_1 = 4$), $\omega_2 = 10^{12}\,\text{s}^{-1}$ (i.e., $m_2 = 12$), and $\Delta\varepsilon'/(m_2 - m_1) = 0.14$. A good agreement between the experimental data and the results of the simple closed-form formula can be seen, which is estimated to be almost within the experimental error.

IV. Numerical Examples

The first example is the propagation of a uniform plane wave in a homogeneous medium, assumed to have the same parameters as FR-4. The wave propagates in the direction of the x-axis. In the complex domain, this propagation is described by the exponential factor $\exp\left(-x\sqrt{-\omega^2(\varepsilon'-j\varepsilon'')\varepsilon_o\mu_o}\right)$, where ε_o and μ_o are the parameters of a vacuum. We assume the wave to be a delta-function of time, centered at t=0 for x=0. We consider the wave at x=1 m, i.e., we evaluate the impulse response. If we take ε'=4.5 and ε"=0.1, independently of frequency, we get a non-causal response, as shown in Figure 5. If we take these parameters to vary with frequency according to the approximations depicted in Figure 4, we get causal responses, as also shown in Figure 5. The differences between the two latter responses directly correspond to the slight differences between the approximation curves in Figure 4, in particular in the GHz region, where the major part of the spectrum is located. The lower ε' from equation (3) results in a somewhat faster pulse propagation, and lower ε" yields smaller losses.

The second example is a microstrip line, produced on FR-4. The dimensions of the line are the same as used to measure the scattering parameters of the line in Section II. The impulse response of the line was measured using the HP 8510B network analyzer (calculated from frequency data in the range 0.05-20 GHz), and also evaluated numerically, assuming the substrate parameters to vary according to eqns. (3) and (5). The excitation waveform of the generator driving the line was taken from the experimental data for the reflection from the open-circuit calibration standard.

The theoretical results were obtained starting from the quasi-static primary parameters of the line. For strip width w=3 mm, strip thickness t=35 μm, substrate thickness h=1.5 mm, real part of the substrate permittivity $\varepsilon' = \varepsilon'_\infty = 4.20$, imaginary part ε"=0.084 (tan δ=0.02), conductor conductivity $\sigma_c = 20\,\text{MS/m}$ (equivalent for copper to include the surface roughness), and reference frequency $f_r = 1\,\text{GHz}$ (for which the primary parameters are evaluated), program LINPAR [20] yields the following primary parameters of the microstrip line: L=295.3 nH/m, C=120.7 pF/m, R=5.29 Ω/m, and G=13.53 mS/m. However, for the evaluation of the transient response, we need the primary parameters as a function of frequency, not only at f_r.

For the purpose of the present analysis, where the major portion of the spectrum is localized in the GHz region, we can assume the skin effect to be fully pronounced, so that the resistance per unit length is given by

$$R(\omega) = R(\omega_r)\sqrt{\frac{\omega}{\omega_r}} \;, \tag{8}$$

where $\omega_r = 2\pi f_r$. The total inductance per unit length, given as the sum of the external and internal inductances, is

$$L(\omega) = L + \frac{R(\omega)}{\omega} \;. \tag{9}$$

The capacitance per unit length of the line (C) depends on the frequency through the relative permittivity. For many practical structures, this dependence can accurately be approximated by a linear function in a wide range of permittivities. This amounts to using a two-term Taylor series, i.e.,

$$C(\varepsilon') \approx C(\varepsilon'_\infty) + \frac{\mathrm{d}C}{\mathrm{d}\varepsilon'}\bigg|_{\varepsilon'=\varepsilon'_\infty} \left(\varepsilon' - \varepsilon'_\infty\right). \tag{10}$$

The derivative $\dfrac{\mathrm{d}C}{\mathrm{d}\varepsilon'}\bigg|_{\varepsilon'=\varepsilon'_\infty}$ can easily be evaluated numerically, by calculating the capacitance for two permittivities. However, we are already using a tool for evaluation of the conductance per unit length (G). The basic approach in program LINPAR is to use an electrostatic analysis, treat the permittivity to be complex, and extract the conductivity from the imaginary part of the resulting complex capacitance. The imaginary part of the complex permittivity is much smaller than the real part, so that from (10) we have

$$-\mathrm{j}\frac{G}{\omega} = \mathrm{j}\,\mathrm{Im}\left\{ C(\varepsilon'_\infty - \mathrm{j}\varepsilon'') \right\} \approx C(\varepsilon'_\infty - \mathrm{j}\varepsilon'') - C'(\varepsilon'_\infty) \approx \frac{\mathrm{d}C}{\mathrm{d}\varepsilon'}\bigg|_{\varepsilon'=\varepsilon'_\infty} \left(-\mathrm{j}\varepsilon''\right), \tag{11}$$

and the required derivative can be readily evaluated from only one run of LINPAR. Both the capacitance and conductance per unit length can be evaluated from eqn. (10) upon introducing the complex relative permittivity from (3) or (5) instead of ε'. Finally, a simple correction was introduced in the phase velocity, according to Reference [21], to include the dispersion of the quasi-TEM mode, which becomes pronounced at frequencies about 10 GHz. The measured and computed data for the pulse response are shown in Figure 6. The agreement is very good, in particular when the dispersion is taken into account.

V. Conclusions

The relative complex permittivity of FR-4 was considered as a function of frequency. Several experimental techniques were used to measure the permittivity in a broad frequency range, from power frequencies up to the microwave region. These data show a decay of the real part with an almost constant slope per frequency decade, while the imaginary part is reasonably independent of the frequency.

The experimental data were fitted by two simple functions. The first function is a series of rational functions with first-order polynomials in denominators. The second function is a logarithm of a bilinear function of the complex frequency. In both cases, a good match with the experimental data was obtained. Both fitting functions yield a causal response in the time domain, as well as good agreement with measured data for the time-domain response.

References

[1]   *Electromagnetic Properties of Materials Program*, NIST web site.

[2]   *Basic of Measuring the Dielectric Properties of Materials*, Application Note 1217-1, Hewlett Packard.

[3]   *Permittivity Measurements of PC Board and Substrate Materials Using the HP 4291A and HP 16453A*, Application Note 1255-3, Hewlett Packard.

[4]   L. S. Napoli, and J. J. Hughes, "A simple technique for the accurate determination of the microwave dielectric constant for microwave integrated circuits", *IEEE Trans. Microwave Theory Tech.*, vol. MTT-19, pp. 664-665, July 1971.

[5]   J. G. Richings, "An accurate experimental method for determining the important properties of microstrip transmission lines", *The Marconi Review*, Fourth Quarter, pp. 209-215, 1974.

[6]   C. H. Riedell, M. B. Steer, M. R. Kay, J. S. Kasten, M. S. Basel, and R. Pomerleau, "Dielectric characterization of printed circuit board substrates", *IEEE Trans. Instrum. Meas.*, vol. IM-39, pp. 437-440, April 1990.

[7]   A. A. Brandt, *Issledovanie Diȉlektrikov na Sverhvìsokih ~astotah*, Moskva: Gos. Izd. Fiz-Mat. Lit., 1963.

[8]   S.-H. Chao, "An uncertainty analysis for the measurement of microwave conductivity and dielectric constant by the short-circuited line method", *IEEE Trans. Instrum. Meas.*, vol. IM-35, pp. 36-41, March 1986.

[9]   L. P. Ligthart, "A fast computational technique for accurate permittivity determination using transmission-line method", *IEEE Trans. Microwave Theory Tech.*, vol. MTT-31, pp. 249-254, March 1983.

[10]   H. A. N. Hejase, "On the use of Davidenko's method in complex root search", *IEEE Trans. Microwave Theory Tech.*, vol. MTT-41, pp. 141-143, January 1993.

[11]   A. M. Nicolson, and G. F. Ross, "Measurement of the intrinsic properties of materials by time domain techniques", *IEEE Trans. Instrum. Meas.*, vol. IM-19, pp. 377-382, November 1970.

[12]   *Measuring Dielectric Constant with the HP 8510 Network Analyzer*, Product Note 8510-3, Hewlett Packard.

[13]   A.-H. Boughriet, Ch. Legrand, and A. Chapoton, "Noniterative stable transmission/reflection method for low-loss material complex permittivity determination", *IEEE Trans. Microwave Theory Tech.*, vol. MTT-45, pp. 52-57, January 1997.

[14]   *Touchstone 1.45*, Westlake Village: EEsof, 1985.

[15]   J. A. Nelder, and R. Mead, "A simplex method for function minimization", *Comp. J.*, no. 7, pp. 308-313, 1965.

[16]   A. R. von Hippel, "Dielectrics and Waves", New York: J. Wiley, 1954.

[17]   Á. M. Poplavko, *Fizika Diȉlektrikov*, Kiev: ViÈa [kola, 1980.

[18]   T. R. Arabi, A. T. Murphy, T. K. Sarkar, R. F. Harrington, and A. R. Djordjević, "On the modeling of conductor and substrate losses in multiconductor, multidielectric transmission line systems," *IEEE Trans. Microwave Theory Tech.*, vol. MTT-39, pp. 1090-1097, July 1991.

[19]   A. R. Djordjević, "SPICE-compatible models for multiconductor transmission lines in Laplace-Transform domain", *IEEE Trans. on Microwave Theory and Techniques*, vol. MTT-45, Part I, pp. 569-579, May 1997.

[20]   A. R. Djordjević, M. B. Baždar, R. F. Harrington, and T. K. Sarkar, *LINPAR for Windows: Matrix Parameters for Multiconductor Transmission Lines, Software and User's Manual*. Norwood, MA: Artech House, 1995.

[21]   W. J. Getsinger, "Microstrip dispersion model", *IEEE Trans. Microwave Theory Tech.*, vol. MTT-21, pp. 34-39, January 1973.

Captions to Figures

Fig. 1.   Raw measured data for the (a) real part (ε') and (b) imaginary part (ε'') of the complex permittivity of FR-4 in the X-band, obtained using various techniques.

Fig. 2.   The real part (ε') and the imaginary part (ε'') of the complex permittivity of FR-4, along with the corresponding loss tangent ($\tan\delta$), in a broad frequency band: compilation of raw measured data, and approximations according to eqn. (2).

Fig. 3.   Equivalent scheme of a parallel-plate capacitor according to (a) eqn. (2), and (b) eqn. (3).

Fig. 4.   (a) The real part (ε') and (b) the imaginary part (ε'') of the complex permittivity of FR-4, along with the corresponding loss tangent ($\tan\delta$) in a broad frequency band: compilation of raw measured data, and approximations according to eqns. (3) and (5).

Fig. 5.   Computed propagated plane-wave impulse through FR-4, for various approximations of the complex permittivity.

Fig. 6.   Impulse response of a microstrip transmission line produced on FR-4: measured, and computed using eqns. (3) and (5).
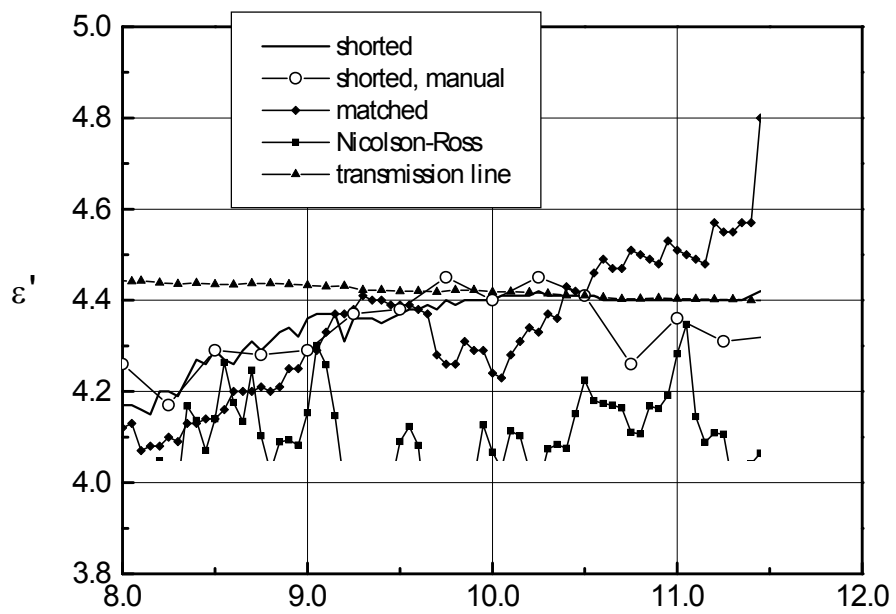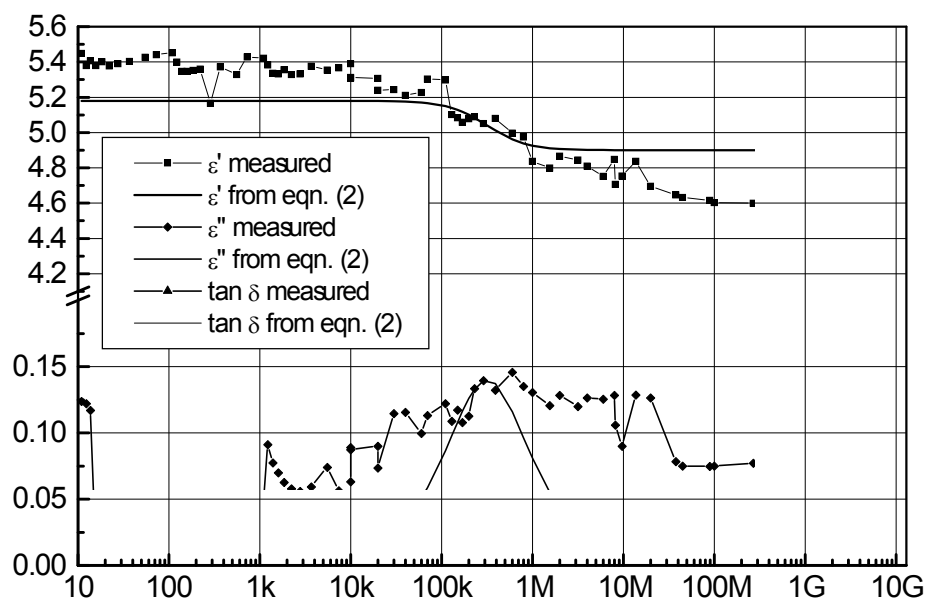
(a)

(b)

Figure 1.

Figure 2.

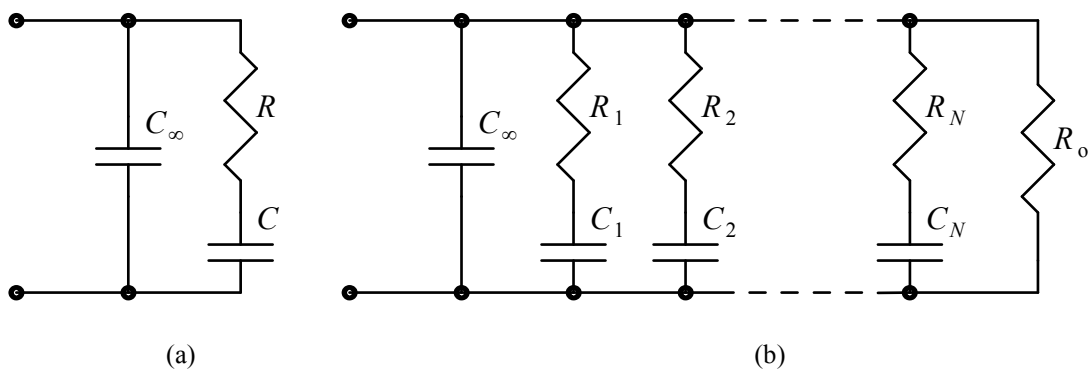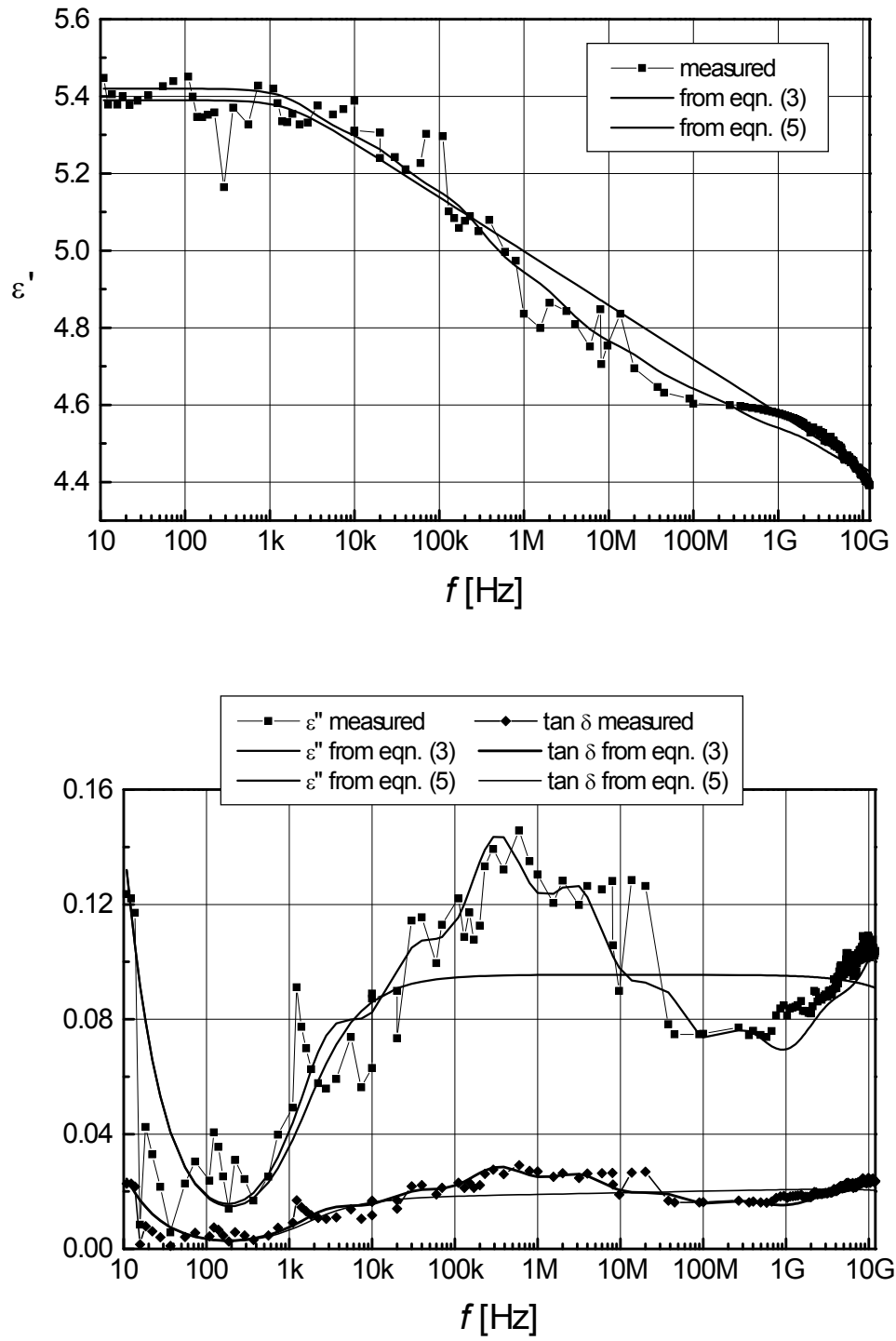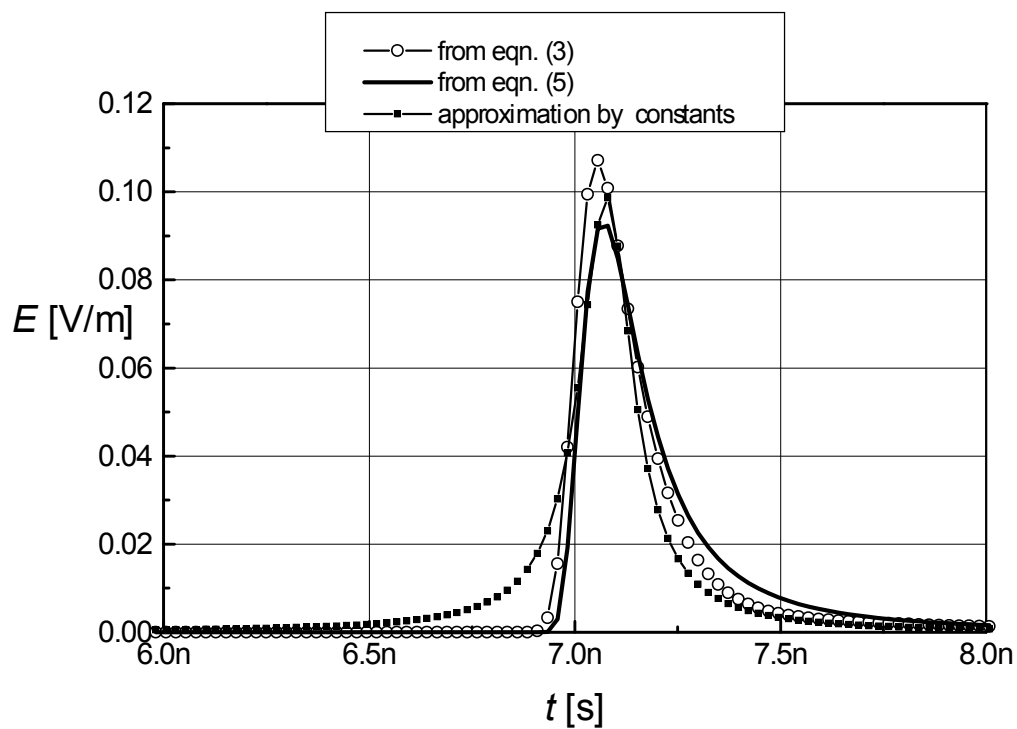(a)   (b)
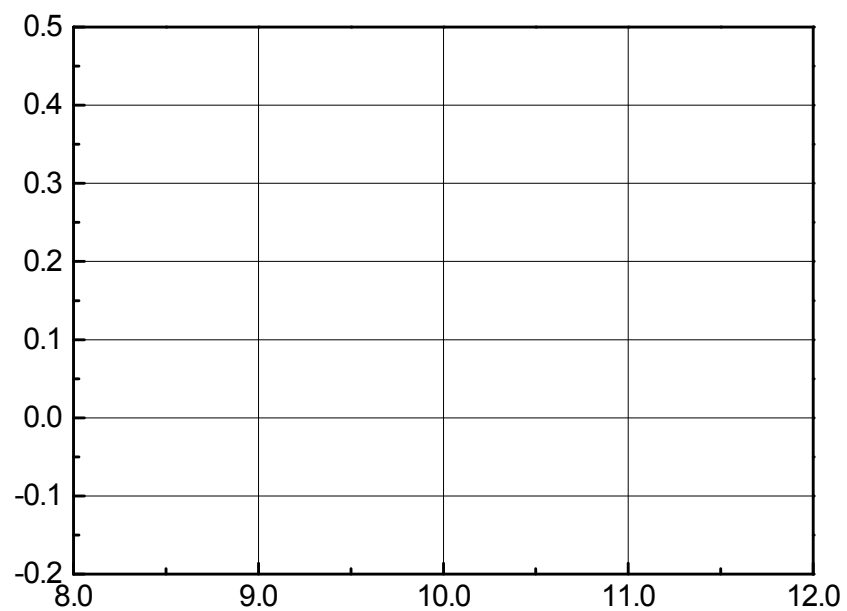
Figure 3.

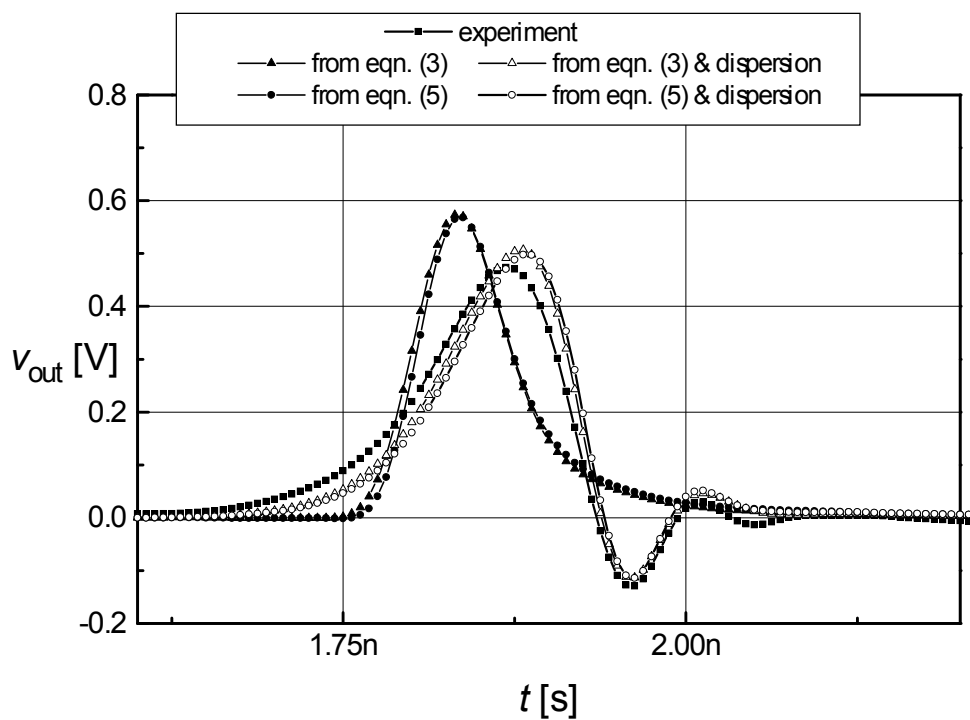Figure 4.

Figure 5.

Figure 6.